Journal of Applied Physics

Influence of structural parameters on organic semiconducting polymer lasers with an external holographic grating as feedback layer

Cite as: J. Appl. Phys. **126**, 093103 (2019); https://doi.org/10.1063/1.5100859
Submitted: 23 April 2019 . Accepted: 14 August 2019 . Published Online: 03 September 2019

Lijuan Liu, Xiaobo Kong, Yanqing Liu, Lin Sun, and Li Xuan

Journal of Applied Physics ARTICLE scitation.org/journal/jap

Influence of structural parameters on organic semiconducting polymer lasers with an external holographic grating as feedback layer

Cite as: J. Appl. Phys. **126**, 093103 (2019); doi: 10.1063/1.5100859
Submitted: 23 April 2019 · Accepted: 14 August 2019 ·
Published Online: 3 September 2019

Lijuan Liu,[1,a)] Xiaobo Kong,[1] Yanqing Liu,[1] Lin Sun,[1] and Li Xuan[2]

AFFILIATIONS

[1]School of Physics and Physical Engineering, Shandong Provincial Key Laboratory of Laser Polarization and Information Technology, Qufu Normal University, 273165 Qufu, China
[2]State Key Laboratory of Applied Optics, Changchun Institute of Optics, Fine Mechanics and Physics, Chinese Academy of Sciences, Changchun 130033, China

[a)]**E-mail:** llj2007weihai@163.com

ABSTRACT

We report on the fabrication and characterization of an organic distributed feedback laser excited from a semiconducting polymer gain layer, poly(2-methoxy-5-(2′-ethyl-hexyloxy)-*p*-phenyl-envinylene) (MEH-PPV). A holographic polymer dispersed liquid crystal grating is fabricated on top of the homogeneous MEH-PPV layer as an external cavity. We established a model to calculate the confinement factor Γ. With the change of laser structural parameters (the refractive index of the grating layer, the film thickness of the MEH-PPV layer, etc.), the confinement factor Γ changes accordingly. It was found that a single longitudinal lasing mode could be observed only when the confinement factor Γ was in a specific range. Choosing a reasonable thickness of gain film and prepolymer with higher refractive index can obtain a lower threshold emission laser.

I. INTRODUCTION

Organic semiconductor lasers (OSLs) have been the subject of numerous investigations for many years mainly due to the advantages of wavelength tunability in the visible range,[1] low cost, and flexibility.[2] These properties make them good candidates for a range of applications including sensing for explosive vapors,[3] high sensitivity spectroscopy,[4] and optical communication.[5] Compared with other types of resonators, distributed feedback (DFB) resonators are compact, can be readily integrated into organic thin films, and can provide a high degree of spectral selection. However, only optical pumping and indirect electrical pumping with cheap inorganic diode lasers[6] or light emitting diodes[7] are possible now. The demonstration of an electrically driven organic laser diode still remains a very challenging task due to some additional loss mechanisms under electrical injection.[8] Therefore, much effort in this field has focused on reducing the thresholds by enhancing the gain medium properties[9] and optimizing the resonant cavities.[10]

Concerning the resonant cavity optimization, many studies investigated on varying the grating period,[11] the grating depth,[12] and the film thickness.[13] The lowest threshold is usually obtained when the organic film thickness is optimized and the emission wavelength becomes close to the peak wavelength of the amplified spontaneous emission (ASE). So far, two kinds of configurations are commonly used: engraving the grating structure directly on the active material[14] or depositing the active medium on the corrugated substrate.[15] In either case, it is difficult to predict the final thickness of the active film and the coupling mechanism is complex. A holographic polymer dispersed liquid crystal (HPDLC) grating layer is one of the most promising external DFB structures since we can control the parameter of the active layer and the HPDLC grating layer separately. A HPDLC grating is prepared in a single-step exposure of a homogeneous mixture of prepolymer/LC mixture to an interference fringe pattern by the photopolymerization induced phase separation (PIPS) method.[11]

In this work, we present the influence of laser structural parameters on the properties of second-order DFB OSL, which

uses a HPDLC grating as the external feedback layer. We also develop a model within the framework of asymmetric slab waveguide theory to characterize the laser structure numerically. The resonant cavity has an influence on the lasing performance through the confinement factor Γ. When Γ is too small (for thinner film case) or too large (for thicker film case), the emission spectra broaden. Only when Γ is in a specific range, a single longitudinal lasing mode can be observed. Therefore, we can optimize the organic laser with external feedback structure better.

II. EXPERIMENTAL

A. Thin film preparation

The MEH-PPV (average molecular weight 120 000; OLED Material Tech.) was dissolved in chlorobenzene (CB) solvent (0.7 wt. %) and stirred for 24 h to ensure sufficient dissolution. Then, the solution was deposited onto a piece of precleaned glass substrate by spin coating for 45 s. The thickness of the MEH-PPV film h was controlled by the spin speed. After spin coating, the MEH-PPV film was heated from room temperature to 120 °C in a vacuum oven. Then, the films were placed at 120 °C for 1 h and slowly cooled to room temperature. The thickness of the MEH-PPV film was investigated by a Dektak Profilometer (KLA Tencor P-16+). The absorption and photoluminescence (PL) spectra were measured by a scanning spectrophotometer (Shimadzu UV-3101; Shimadzu Corp., Japan) and a fluorescence spectrophotometer (Hitachi F-4500; Hitachi, Ltd., Tokyo, Japan), respectively.

B. HPDLC grating fabrication

The materials adopted in the mixture for HPDLC grating were nematic LC TEB30A ($n_o = 1.522$, $n_e = 1.692$, $\Delta n = 0.170$, Slichem, 28 wt. %), *N*-vinylpyrrolidone (NVP, Sigma-Aldrich, 10 wt. %) as a solvent and a chain extender, coinitiator *N*-phenylglycine (NPG, Sigma-Aldrich, 1.5 wt. %), photo-initiator Rose Bengal (RB, Sigma-Aldrich, 0.5 wt. %), and the monomer (60 wt. %). To check the effect of refractive index (RI), dipentaerythritol hydroxyl pentaacrylate (DPHPA, Aldrich, 30 wt. %) and phthalic diglycol diacrylate (PDDA, Aldrich, 30 wt. %) were adopted in mixture A, while only bisphenol F ethoxylate (2 EO/phenol) diacrylate (BPFEDA, Aldrich, 60 wt. %) was prepared in mixture B. The mixture was stirred in dark at room temperature for 12 h and injected into the empty cells by capillary action. The cell was prefabricated by combining the MEH-PPV coated glass substrate with a bare glass substrate. The cell gap, i.e., the thickness of the HPDLC grating, was controlled by a Mylar spacer at 6 μm. Then, the cell underwent holographic photocuring by two coherent s-polarized laser beams from a 532 nm Nd:YAG laser.[11,16–18] The schematic optical setup is shown in Fig. 1(a). HPDLC gratings with different periods can be derived by

$$\Lambda = \frac{\lambda_{532}}{2\sin(\theta/2)}, \tag{1}$$

where θ is the intersection angle between the two coherent beams. The intensity of each recording beam was 3.7 mW/cm^2 and the exposure time was 5 min. Different samples were prepared, as shown in Table I. Samples **a1**–**a6** and **a2***** were made from mixture A, and samples **b1**–**b6**, **b3***, and **b4*** were made from mixture B. To compare the effect of the film thickness, the film thickness of samples was varied from 60 nm to 200 nm. The period of the gratings for samples **a1**–**a6** and **b1**–**b6** was chosen at 395 nm. For samples **a2***, **b3***, and **b4***, the periods of the

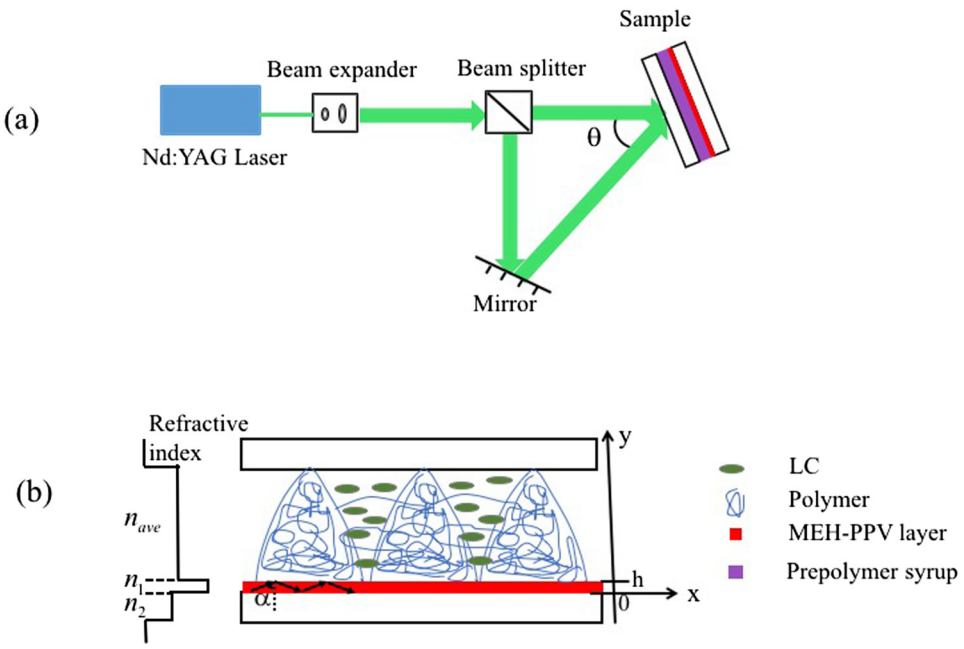

FIG. 1. (a) Optical setup for fabrication HPDLC grating layer and (b) schematic illustration of the waveguide DFB structure.

TABLE I. Illustration and properties of samples. $P_{grating}$, $P_{MEH-PPV}$, and P_{glass} are the percentages of mode energy distribution in the grating layer, the MEH-PPV layer, and the glass substrate, respectively. We will discuss them in Sec. III B.

Sample No.	Mixture	h(nm)	$P_{grating}$(%)	$P_{MEH-PPV}$(%)	P_{glass}(%)	$P_{grating}/P_{MEH-PPV}$
a1	A	60	46.3	18.4	35.3	2.52
a2	A	70	42.3	23.7	34.0	1.78
a2*	A	70	42.0	24.1	33.9	1.74
a3	A	80	38.8	28.9	32.3	1.34
a4	A	90	35.6	34.0	30.4	1.05
a5	A	100	32.7	39.0	28.3	0.84
a6	A	200	14.3	72.7	13.0	0.20
b1	B	60	57.6	16.3	26.1	3.53
b2	B	70	51.0	21.8	27.2	2.34
b3	B	80	45.8	27.2	27.0	1.68
b3*	B	80	46.1	26.7	27.2	1.73
b4	B	90	41.1	32.5	26.4	1.26
b4*	B	90	41.8	31.5	26.7	1.33
b5	B	100	37.6	37.4	25.0	1.00
b6	B	200	15.9	71.7	12.4	0.22

gratings were carefully chosen at 397.8 nm, 391.8 nm, and 389.0 nm, respectively.

C. Optical pumping

The sample was optically pumped by a Q-switched frequency-doubled Nd:YAG laser (532 nm, 2 Hz, 8 ns). The pump beam was shaped into a narrow stripe (5 mm by 0.1 mm) by a cylindrical lens and an adjustable slit. For a real-time detection of pump energy, a beam splitter was placed between the adjustable slit and the sample. One stripe was directed into an energy meter, and the other stripe was incident onto the sample at an angle of 60° with respect to the glass substrate. The vertical laser emission was detected and measured by a fiber coupled spectrometer (with a resolution of ~0.25 nm) and an energy meter (LabMax-TOP; Coherent Inc., Santa Clara, CA, USA) respectively.

III. RESULTS AND DISCUSSION

A. Optical properties of the MEH-PPV films

The surface morphology properties of the MEH-PPV films were investigated by a tapping mode Atomic Force Microscope (AFM, BRUKER Multimode 8). Figure 2 shows three dimensional topographic images of MEH-PPV films with different film thicknesses. The root mean square (RMS) value, which represents the degree of the surface roughness, varied from 0.317 nm to 1.253 nm with the film thickness increased from 60 nm to 200 nm. The thinner the film thickness the smoother the film surface. The ASE, absorption, and PL spectra of the MEH-PPV film annealing at 120 °C were demonstrated in Fig. 3(a). All of the spectra had a slightly red shift compared with the MEH-PPV film with no annealing treatment due to the decrease of $\pi \rightarrow \pi^*$ energy gap.[16,19] For ASE measurement, each sample was irradiated under a single laser beam from a Nd:YAG laser (532 nm, 20 mW/cm^2) for 10 min. This homogeneous illumination would result in a polymer dispersed liquid crystal (PDLC) layer.[11] The ASE peak was located at 623 nm, and the full width at half maximum (FWHM) was about 8 nm. Figure 3(b) shows the dependence of PL intensity on the film thickness. Since MEH-PPV is a highly absorbing material, light will be absorbed rapidly with an increase of film thickness, and PL intensity will no longer increase after a certain film thickness (100 nm for MEH-PPV).

B. Waveguide characterization and confinement factor calculation

In earlier works,[20] we have demonstrated a HPDLC grating with polymer scaffolding morphology. The phase-separated LCs are well aligned along the grating vector as shown in Fig. 1(b); thus, the RI of the LCs is n_o. The phase separation degrees σ are 0.12 for samples **a1**–**a6** and 0.13 for samples **b1**–**b6**, respectively, which are measured by a birefringence test.[21] For feedback light with a TE polarization propagating along the grating vector, the average grating RI n_{ave} can be calculated by

$$n_{ave} = [n_p^2 \times \phi_p + n_o^2 \times \sigma + n_{iso}^2 \times (1 - \phi_p - \sigma)]^{1/2}, \quad (2)$$

where n_p is the RI of pure polymer (1.525 for mixture A, 1.57 for mixture B), ϕ_p is the volume proportion of pure polymer in the grating, which is 0.7 in this work,[20] $n_{iso} = (2/3n_o^2 + 1/3n_e^2)^{1/2}$, which is the RI of dissolved LCs in the polymer matrix. According to Eq. (2), the average RI of HPDLC grating layer can be known (1.535 for samples **a1**–**a6** and **a2***, 1.566 for samples **b1**–**b6**, **b3***, and **b4***).

Considering that the organic laser wavelength λ follows the asymmetric TE waveguide equation,[22]

$$\frac{2\pi}{\lambda} n_1 h \cos\alpha - \arctan\frac{\sqrt{n_1^2 \sin^2\alpha - n_2^2}}{n_1 \cos\alpha} - \arctan\frac{\sqrt{n_1^2 \sin^2\alpha - n_{ave}^2}}{n_1 \cos\alpha} = 2M\pi, \quad (3)$$

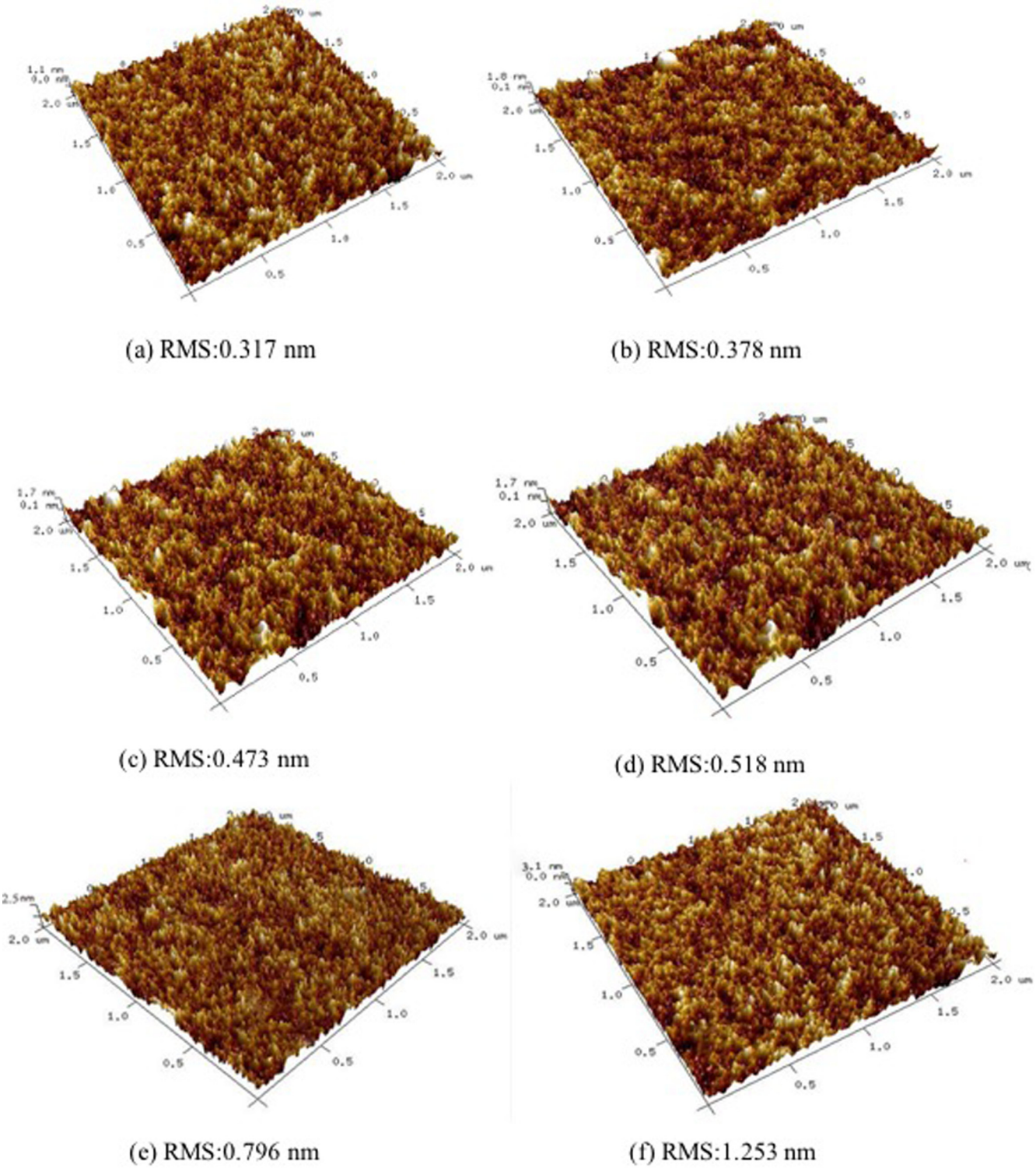

FIG. 2. AFM images of the MEH-PPV surface of different film thicknesses (a) 60 nm, (b) 70 nm, (c) 80 nm, (d) 90 nm, (e) 100 nm, and (f) 200 nm.

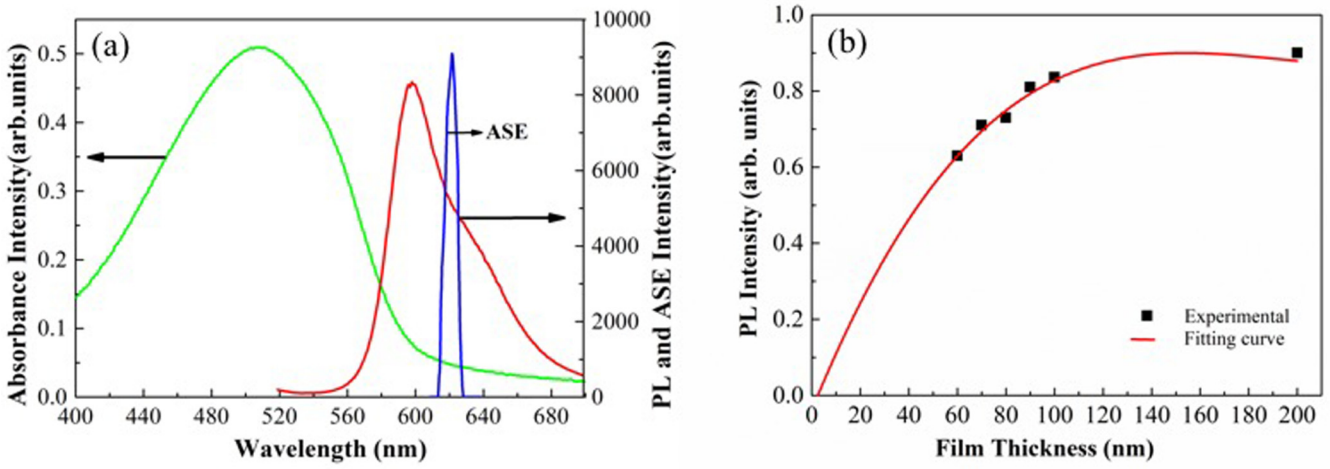

FIG. 3. (a) ASE, absorption, and PL spectra of the MEH-PPV film and (b) PL intensity as a function of film thickness: symbols are experimental data and the full line is the corresponding fitting curve.

where h is the MEH-PPV film thickness, α is the angle of incidence for laser mode, M is the mode number, and n_1(1.90) and n_2(1.516) are the RI of MEH-PPV films and glass substrates, respectively [as shown in Fig. 1(b)].

The electric fields in these three regions can be expressed by

$$E_y(x) = \begin{cases} A_0 \exp[-\alpha_0(y-h)] & y \geq h \\ A_1 \cos(k_{1x}y - \varphi) & h \geq y \geq 0 \\ A_2 \exp(\alpha_2 & y)y \leq 0 \end{cases}, \quad (4)$$

where $\alpha_0 = \sqrt{\beta^2 - k_0^2 n_0^2}$, $k_{1x} = \sqrt{k_0^2 n_1^2 - \beta^2}$, $\alpha_2 = \sqrt{\beta^2 - k_0^2 n_2^2}$, and $k_0 = 2\pi/\lambda$. The propagation constant β is the projection of the wave vector k_0 along the propagation direction ($\beta = k_0 n_1 \sin\alpha$). According to the boundary conditions for waveguide, the electric fields in these three regions for different film thicknesses can be solved.

The percentages of mode energy distribution in the grating layer, the MEH-PPV layer, and the glass substrate are calculated using the following expressions:

$$P_{grating} = \frac{\int_h^{+\infty} E_y^2(x,y,z)dx}{\int_{-\infty}^{+\infty} E_y^2(x,y,z)dx},$$

$$P_{MEH-PPV} = \frac{\int_0^h E_y^2(x,y,z)dx}{\int_{-\infty}^{+\infty} E_y^2(x,y,z)dx}, \quad (5)$$

$$P_{glass} = \frac{\int_{-\infty}^0 E_y^2(x,y,z)dx}{\int_{-\infty}^{+\infty} E_y^2(x,y,z)dx}.$$

The confinement factor Γ is defined as $\Gamma = P_{grating}/(P_{grating} + P_{MEH-PPV} + P_{glass})$, since $P_{grating} + P_{MEH-PPV} + P_{glass} = 1$ and $\Gamma = P_{MEH-PPV}$. According to Eqs. (3)–(5), we can calculate the mode energy distribution for samples with different film thicknesses in Table I.

C. Effect of film thickness on laser performance

When optically pumped, the laser emission occurred from our samples. The laser wavelength λ satisfies the Bragg condition,

$$m\lambda = 2n_{eff}\Lambda, \quad (6)$$

where n_{eff} is the effective RI of the laser mode and m is the Bragg order, which was selected as 2 in this work. There were two output lasing beams with equal intensity emitted from the normal direction of the glass substrate. The emitted laser is totally TE polarized. Figure 4 shows the experimental emission spectra of the samples with different MEH-PPV thicknesses.

For samples **a1**, **b1**, and **b2**, the percentage of mode energy distribution in the MEH-PPV layer is low (about 20%) as shown in Table I. Lasing threshold is difficult to achieve due to the inefficient utilization of the gain volume, so the emission spectra become wide. For samples **a4–a6** and **b5–b6**, although more than 35% light is bounded in the MEH-PPV layer, the percentage of mode energy distribution in grating is decreased. There is no sufficient light spread into the grating layer to interact with the periodic structure, and the bounded light also exhibited wide spectrum. A single longitudinal lasing mode can be observed in samples **a2–a3** and **b3–b4**, since the energy is well balanced in the distribution of the grating and the gain medium layer. Γ increases with the film thickness, and the value of Γ is between 0.22 and 0.33. Specifically, the value of $P_{grating}/P_{MEH-PPV}$ remains between 1.2 and 1.8 regardless of other parameters.

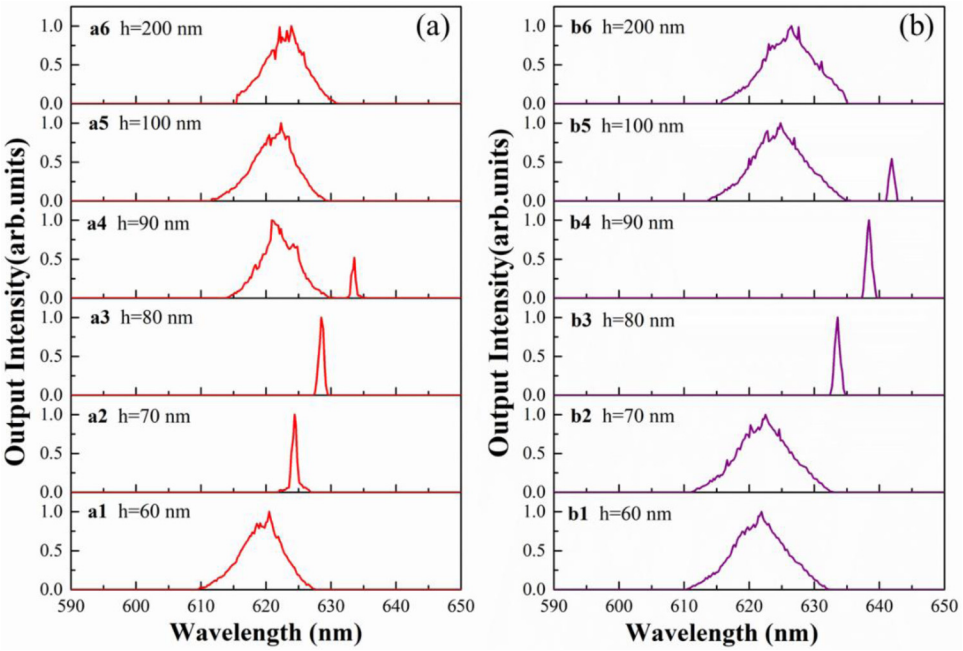

FIG. 4. Emission spectra of samples for (a) **a1**–**a6** and (b) **b1**–**b6**, respectively.

Figure 5 shows the calculated lasing wavelength and effective RI value for different film thicknesses, obtained by solving Eqs. (3) and (6). The hollow squares and hollow circles are the experimental data of lasing wavelength and effective RI value. The experimental data are in good agreement with the theoretical data. The effective RI n_{eff} value is higher for the sample with thicker films, resulting in a red shift for laser emission. For the samples with the same film thickness, the higher the RI of the prepolymer, the higher the effective RI of the mode.

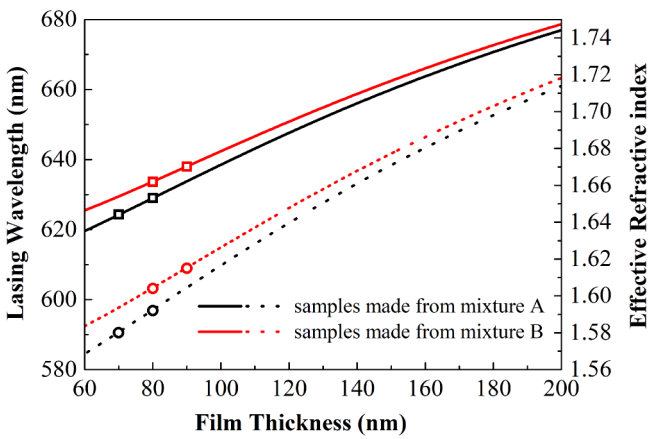

FIG. 5. Lasing wavelength (solid line) and effective RI value (dotted line) as a function of MEH-PPV film thickness: symbols are experimental data.

The spectra of samples **a2***, **a3**, **b3***, and **b4*** were measured at a pump energy of 0.70 μJ, as shown in Fig. 6(a). The lasing peaks are located at 628.8 nm, 628.5 nm, 628.5 nm, and 628.5 nm, respectively. The lasing peaks are close to the peak of ASE where the net gain is the highest. Lasing with a narrow linewidth was observed, and their FWHM was 0.5–0.7 nm. Figure 6(b) shows the dependence of output lasing energy on the pump energy for these samples. The output lasing energy increases slowly with the pump energy at the initial stage, and then the output lasing energy increases abruptly when the pump energy reaches the lasing threshold. The slope efficiencies of samples **a2***, **a3**, **b3***, and **b4*** are 6.03%, 6.35%, 6.21%, and 6.52%, respectively. The thresholds of the samples are 0.24 μJ, 0.18 μJ, 0.20 μJ, and 0.16 μJ, respectively. For the same value of RI, an increase in the thickness (samples **a2***–**a3** and samples **b3***–**b4***) is followed by an increase in Γ and a decrease in threshold. However, for the same value of thickness, an increase in the RI (samples **a3**–**b3***) is followed by a decrease in Γ and an increase in slope threshold. Sample **b4*** has the highest slope efficiency and the lowest laser threshold. The performance of laser emitted from **b4*** can be attributed to its higher absorption due to thicker films and less mode energy distribution in the glass layer. These results show that the laser can have better performance by choosing a reasonable thickness of gain film and prepolymer with higher RI. A reasonable thickness of gain film can allow sufficient light spread into the grating layer to interact with the periodic structure as well as obtain enough gain. Using prepolymer with higher RI to fabrication HPDLC grating can reduce the percentage of mode energy distribution in the glass substrate, which is useless for lasing output performance. Therefore, the lasing threshold and conversion efficiency can be enhanced in this work.

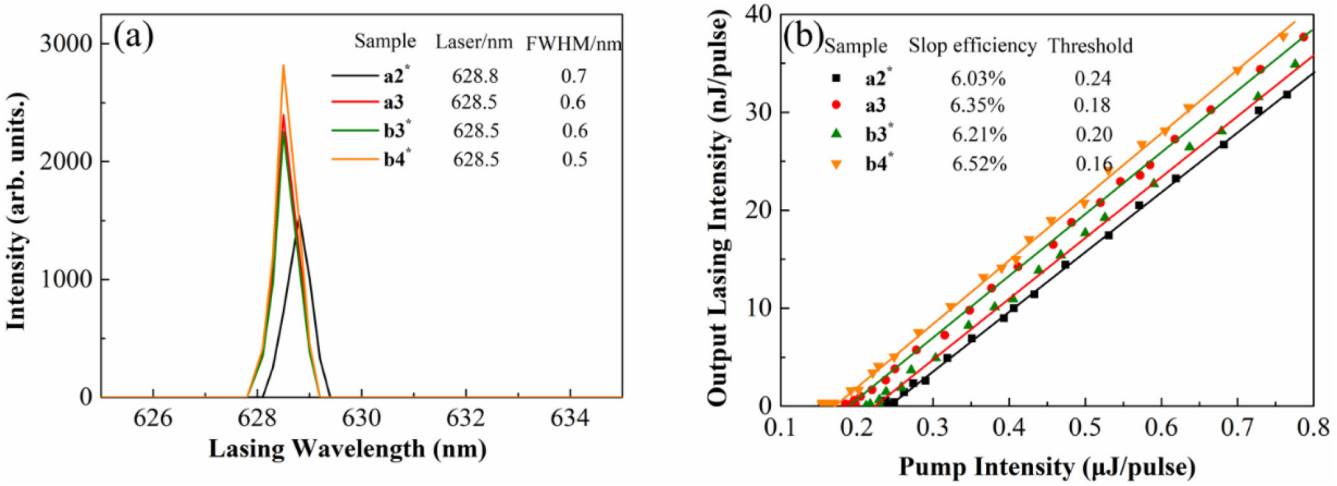

FIG. 6. (a) Lasing spectra at 0.70 μJ and (b) lasing output intensity as a function of pump intensity for samples **a2***, **a3**, **b3***, and **b4***.

IV. CONCLUSIONS

In conclusion, we have fabricated and characterized the second-order DFB laser based on a HPDLC transmission grating. The organic lasing behaviors vary with the laser structural parameters. In order to better understand these results, we developed a simple model, and the properties of the resonant cavity were investigated through the calculation of confinement factor Γ. It was found that a single longitudinal lasing mode could be observed only when the confinement factor Γ was in a specific range. The numerical characterization results are compared to the experimental ones and are in good agreement. This work will give more understanding of film thickness on organic DFB laser performance and make contribution to the development of organic semiconducting polymer lasers.

ACKNOWLEDGMENTS

The authors would like to acknowledge financial support from the National Natural Science Foundation of China (NSFC) (Grant No. 51702185) and Natural Science Foundation of Shandong Province (Grant Nos. ZR2017BEM029 and ZR2017MD019).

REFERENCES

[1]O. Mhibik, T. Leang, A. Siove, S. Forgeta, and S. Chénais, Appl. Phys. Lett. **102**, 041112 (2013).
[2]J. Herrnsdorf, B. Guilhabert, Y. Chen, A. L. Kanibolotsky, A. R. Mackintosh, R. A. Pethrick, P. J. Skabara, E. Gu, N. Laurand, and M. D. Dawson, Opt. Express **18**, 25535 (2010).
[3]Y. Yang, G. A. Turnbull, and I. D. W. Samuel, Adv. Funct. Mater. **20**, 2093–2097 (2010).
[4]T. Woggon, S. Klinkhammer, and U. Lemmer, Appl. Phys. B **99**, 47–51 (2010).
[5]J. Clark and G. Lanzani, Nat. Photonics **4**, 438–446 (2010).
[6]C. Karnutsch, M. Stroisch, M. Punke, U. Lemmer, J. Wang, and T. Weimann, IEEE Photon. Tech. Lett. **19**, 741–743 (2007).
[7]Y. Yang, G. A. Turnbull, and I. D. W. Samuel, Appl. Phys. Lett. **92**, 163306 (2008).
[8]C. Gärtner, C. Karnutsch, U. Lemmer, and C. Pflumm, J. Appl. Phys. **101**, 023107 (2007).
[9]G. Tsiminis, Y. Wang, P. E. Shaw, A. L. Kanibolotsky, I. F. Perepichka, M. D. Dawson, P. J. Skabara, G. A. Turnbull, and I. D. W. Samuel, Appl. Phys. Lett. **94**, 243304 (2009).
[10]A. S. D. Sandanayaka, K. Yoshida, M. Inoue, C. Qin, K. Goushi, J. C. Ribierre, T. Matsushima, and C. Adachi, Adv. Opt. Mater. **4**, 834 (2016).
[11]L. Liu, W. Huang, Z. Diao, Z. Peng, Q. Q. Mu, Y. Liu, C. Yang, L. Hu, and L. Xuan, Liq. Cryst. **41**, 145–152 (2013).
[12]V. Navarro-Fuster, I. Vragovic, E. M. Calzado, P. G. Boj, J. A. Quintana, J. M. Villalvilla, A. Retolaza, A. Juarros, D. Otaduy, S. Merino, and M. A. Dıaz-Garcıa, J. Appl. Phys. **112**, 043104 (2012).
[13]F. Bencheikh, A. S. D. Sandanayaka, T. Matsushima, J. C. Ribierre, and C. Adachi, J. Appl. Phys. **121**, 233107 (2017).
[14]I. D. W. Samuel and G. A. Turnbull, Chem. Rev. **107**, 1272–1295 (2007).
[15]G. Heliotis, R. Xia, D. D. C. Bradley, G. A. Turnbull, I. D. W. Samuel, P. Andrew, and W. L. Barnes, J. Appl. Phys. **96**, 6959 (2004).
[16]G. Zhang, Q. Wang, Y. Liu, J. Ma, Z. Peng, L. Yao, D. Li, C. Yang, Q. Mu, Z. Cao, and L. Xuan, Org. Electron. **43**, 148–155 (2017).
[17]L. Liu, G. Zhang, X. Kong, Y. Liu, and L. Xuan, J. Phys. D Appl. Phys. **51**, 045103 (2018).
[18]L. Liu, X. Kong, Q. Wang, Y. Liu, and L. Xuan, J. Mater. Chem. C **6**, 9517–9522 (2018).
[19]G. Zhang, L. Liu, M. Liu, Y. Liu, Z. Peng, L. Yao, Q. Wang, S. Wang, Z. Cao, J. Ma, and L. Xuan, Opt. Mater. Express **6**, 3320 (2016).
[20]W. Huang, Y. Liu, Z. Diao, C. Yang, L. Yao, J. Ma, and L. Xuan, Appl. Opt. **51**, 4013 (2012).
[21]W. Huang, Q. Liu, L. Xuan, and L. Chen, Appl. Phys. B **117**, 1065–1071 (2014).
[22]K. Okamoto, *Fundamentals of Optical Waveguides* (Academic Press, Burlington, 2010).